# Bayesian Optimization of an RF Inductively Coupled Gridded Argon Ion Thruster: Effects of Geometry, RF Power, and Realistic Performance Constraints

Lucas Sekiguchi Crisantemo[1], Rodrigo Sávio Pessoa[1] and Argemiro Soares da Silva Sobrinho[1]
[1]Instituto Tecnológico de Aeronáutica, São José dos Campos/SP - Brazil

***Abstract*— This work presents the numerical optimization of a radio-frequency (RF) inductively coupled plasma gridded ion thruster using argon. A corrected zero-dimensional global model computed plasma and thrust-related quantities, while Bayesian optimization explored reactor diameter, length, and RF power. Two correction layers avoided overly optimistic predictions: a Child–Langmuir current-extraction limit and a realistic system-level penalty including beam, grid, power-processing-unit, and neutralizer efficiencies, with a commercial thrust-to-power cap of $45\,\mathrm{mN/kW}$. The geometry-only study at $900\,\mathrm{W}$ indicates that larger diameters and shorter lengths favor thrust. In the three-variable optimization, the best Child–Langmuir-limited point occurrs at $\mathrm{D} = 18\,\mathrm{cm}$, $\mathrm{L} = 5\,\mathrm{cm}$, and $\mathrm{P_{RF}} \approx 765\,\mathrm{W}$, yielding $63.6\,\mathrm{mN}$; after the realistic penalty, the best point became $45\,\mathrm{mN}$ at $1\,\mathrm{kW}$. Comparison with the ArianeGroup RIT family, QinetiQ T5/T6, and NASA NEXT shows that the penalized model falls within a commercially plausible gridded-ion-engine envelope.**

***Keywords*— Argon plasma, ion thruster, Bayesian optimization.**

## I. Introduction

Electric propulsion is increasingly relevant for orbit raising, station keeping, and deep-space missions due to its high specific impulse and low propellant consumption [1]. Among electric propulsion systems, gridded ion engines are especially attractive because they provide stable and efficient low-thrust operation. A particular class of these devices employs radio-frequency (RF) plasma generation, which removes the need for an internal cathode in the discharge stage and is exemplified by the ArianeGroup RIT family. At the same time, Kaufman-type gridded ion engines such as the QinetiQ T5 and T6 and the NASA NEXT thruster define important reference levels in terms of thrust, power, and thrust-to-power ratio.

Although xenon remains the dominant propellant in commercial gridded ion engines due to its favorable ionization characteristics and high atomic mass, alternative propellants have attracted increasing interest in recent years. Among them, argon represents a promising candidate because of its low cost, wide availability, and compatibility with radio-frequency plasma generation systems which reduces operational costs and facilitates scalability and experimental development of electric propulsion technologies when compared to xenon or other propellants. In addition to economic advantages, argon plasmas exhibit favorable ionization pathways associated with excited and metastable states. These long-lived excited states act as intermediate energy reservoirs and enable stepwise ionization mechanisms, effectively reducing the energy required to generate ions after initial excitation events [2].

Table I summarizes representative characteristics of selected propellants for electric propulsion and highlights the trade-offs between ionization requirements, propellant mass, and economic accessibility.

Table I
Representative characteristics of selected ion-thruster propellants

| Propellant | Atomic mass (u) | First ionization energy (eV) | Relative cost |
|---|---|---|---|
| Xenon | 131.3 | 12.13 | High |
| Krypton | 83.8 | 14.00 | Medium |
| Argon | 39.9 | 15.76 | Low |
| Iodine[1] | 126.9 | 10.45 | Low–Medium |

Compared with xenon and iodine, argon requires higher ionization energy but benefits from low cost, broad availability, and favorable excitation–ionization pathways represented in Table II.

Table II
Representative ionization thresholds in the argon chemistry

| Process | Threshold (eV) |
|---|---|
| $Ar \rightarrow Ar^+$ | 15.76 |
| $Arm \rightarrow Ar^+$ | 4.43 |
| $Arr \rightarrow Ar^+$ | 3.96 |
| $Arp \rightarrow Ar^+$ | 2.26 |

Although the physics of ion thrusters is well established, design optimization remains a multiparametric problem. Changes in chamber diameter and length modify discharge volume, wall area, plasma density, wall losses, inductive coupling, and extraction conditions. Likewise, RF power strongly affects plasma production but may lead to non-extractable ion

Lucas Sekiguchi Crisantemo, lucasekiguchi@gmail.com; Rodrigo Sávio Pessoa, rodrigospessoa@gmail.com; Argemiro Soares da Silva Sobrinho, argemirosss@gmail.com.

[1]Iodine is stored and fed as molecular vapor ($I_2$), requiring a thermally controlled sublimation system distinct from the pressurized-gas feed used for $Xe$ and $Ar$; the ionization energy listed refers to the atomic species produced after dissociation.

current if the Child–Langmuir limit is exceeded. Because a full parametric sweep is expensive and nonlinear, Bayesian optimization is a suitable strategy to guide the search for high-performance designs with a limited number of model evaluations.

The objective of this paper is to present a compact scientific assessment of the developed workflow: (i) a corrected global model of an RF inductively coupled gridded argon ion thruster; (ii) Bayesian optimization of reactor diameter, reactor/coil length, and RF power; and (iii) a realistic comparison against representative commercial gridded ion engines.

## II. Model and methods

The discharge chamber was modeled as a cylindrical reactor of radius R and length L. The global model includes neutral argon, positive ions, excited argon states, electron energy balance, gas energy balance, wall losses, and an RF inductive coupling model [3]. The model resolves the population balance of two metastable/resonant 4s levels ($Ar^m$, $Ar^r$) and one 4p-derived level ($Ar^p$) individually, each governed by its own rate equation and coupled through electron-impact excitation, de-excitation (superelastic collisions), radiative decay, and stepwise-ionization reactions, as summarized in Table II. The aggregate effect of this excited-state network on the electron energy balance is captured through the collisional energy term $\epsilon c(X)$, following the formulation of Magaldi et al. [2]. While the global (0-D) nature of the model does not resolve spatial gradients in excited-state density, the temporal evolution of each excited population is tracked individually within the volume-averaged balance.

For the geometry study, the design variables were the internal diameter $D = 2R$ (6–18 cm), the reactor/coil length $L$ (5–20 cm), and the RF power $P_{RF}$ (200–1200 W). The coil radius was linked to the chamber radius through a constant clearance of 1 cm, and the number of turns was fixed at $N = 5$.

To keep the operating pressure consistent with the nominal 2 mTorr condition, the inlet neutral source term was updated for each geometry according to the neutral flow expression

$$Q_0 = \frac{n_g v_g A_g}{4} \tag{1}$$

where $n_g$ is the neutral density, $v_g$ is the thermal neutral speed, and $A_g$ is the neutral-exit area. The coil inductance was updated as

$$L_{coil} = \frac{\mu_0 \pi R_c^2 N^2}{L} \tag{2}$$

where $R_c$ is the mean coil radius. Bayesian optimization was implemented with Gaussian-process regression and Expected Improvement [4]. In addition to the raw thrust, a Child–Langmuir-limited thrust was defined. When the predicted extracted ion current density $J_i$ exceeded the Child–Langmuir limit $J_{CL}$, the ion-thrust contribution was reduced proportionally while the neutral-thrust contribution was preserved:

$$T_{CL} = \frac{T_i J_{CL}}{J_i} + T_g, \quad if \;\; J_i > J_{CL} \tag{3}$$

$$T_{CL} = T_{total}, \quad if \;\; J_i \leq J_{CL} \tag{4}$$

A second engineering correction was then applied to obtain a realistic performance metric

$$T_{real} = min(T_{CL}\eta_{beam}\eta_{grid}\eta_{PPU}\eta_{neut}, 45\,\mathrm{PkW}) \tag{5}$$

with $\eta_{beam} = 0.90$, $\eta_{grid} = 0.95$, $\eta_{PPU} = 0.92$, and $\eta_{neut} = 0.90$, yielding a global factor $\eta_{global} = 0.70794$. The term 45 PkW imposes an upper commercial envelope of 45 mN/kW for gridded ion engines.

## III. Results and Discussion

In the geometry-only optimization at 900 W, the Bayesian map indicated a clear tendency toward higher thrust for larger diameters and shorter reactor lengths. The best geometry found in this study was $D = 18.0$ cm and $L = 5.0$ cm, with a raw thrust of 104.9 mN, an electron temperature of 3.76 eV, a gas temperature of 315.5 K, and an RF coupling efficiency $\eta_{ICP} = 0.813$. As shown in Fig. 1, the uncertainty map confirms that the Gaussian-process surrogate rapidly identified the most promising region of the design space.

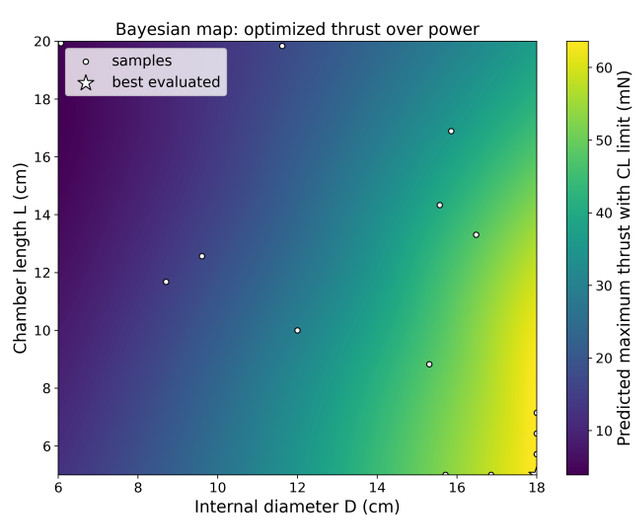


Fig. 1. Bayesian map of predicted maximum thrust in the D–L space after optimization over RF power.

The favorable region identified by the optimizer can also be interpreted from the plasma kinetics represented in the reaction mechanism. Since the model includes excitation and

ionization pathways involving metastable and electronically excited argon populations, absorbed RF power contributes not only to direct ion generation but also to the accumulation of intermediate energetic states.

The favorable region identified by the optimizer is consistent with the role of the excited-state network described in Section II. To quantify this contribution, the complete chemistry (retaining $Ar^r$ and $Ar^p$) was compared against a reduced set in which both levels — and every reaction involving them — were removed, leaving only the ground state, the ion, and the metastable level. Table III reports the steady-state results at $P_{RF} = 900\,\mathrm{W}$ and the reference geometry.

Table III
EFFECT OF CHEMISTRY COMPLEXITY ON STEADY-STATE PLASMA AND THRUST AT $P_{RF} = 900\,\mathrm{W}$, REFERENCE GEOMETRY.

| Quantity | Complete | Reduced | $\Delta$ |
|---|---|---|---|
| $T_e$ (eV) | 3.525 | 3.830 | +8.7% |
| $n_e$ ($\mathrm{m}^{-3}$) | $1.099 \times 10^{18}$ | $1.257 \times 10^{18}$ | +14.4% |
| Total thrust (mN) | 41.5 | 49.6 | +19.5% |
| $\eta_{ICP}$ | 0.557 | 0.561 | +0.7% |

Removing the resonant and 4p levels eliminates two electron-energy-loss channels (excitation to $Ar^r/Ar^p$ and the associated radiative cascade) while leaving the metastable-mediated stepwise pathway of Table II intact. The reduced chemistry therefore channels a larger fraction of the absorbed power directly into ionization, which results in higher equilibrium values of $T_e$ and $n_e$ and a predicted thrust increase of approximately 20%. This indicates that the geometric preference for larger diameters and shorter lengths — which lowers the relative wall-loss area and leaves more power available for the excitation-ionization network — is reinforced, not merely paralleled, by the excited-state kinetics resolved in the model.

From a plasma-chemistry perspective, these operating trends are also compatible with the presence of intermediate excitation pathways represented in the reaction mechanism. Because the model includes metastable and electronically excited argon states, part of the absorbed RF energy contributes to the accumulation of excited populations before conversion into ion current. This effect may reduce the effective energetic burden associated with direct ionization and contribute to sustaining discharge performance across the optimized operating region.

When RF power was added as a third design variable, the Bayesian optimizer converged toward the same high-diameter, short-length region. The best Child–Langmuir-limited point was obtained at $D = 18.0\,\mathrm{cm}$, $L = 5.0\,\mathrm{cm}$, and $P_{RF} = 765\,\mathrm{W}$, resulting in a raw thrust of $90.0\,\mathrm{mN}$ and a corrected thrust $T_{CL} = 63.6\,\mathrm{mN}$. The corresponding current-over-limit ratio was $\frac{J_i}{J_{CL}} = 1.42$, which illustrates why the extraction constraint is essential. Without this correction, the model would systematically overestimate practical thrust in the most aggressive operating conditions. Fig. 2 maps the RF power that maximizes the Child–Langmuir-limited thrust across the explored D–L space, highlighting how the optimal power decreases as the chamber length increases.

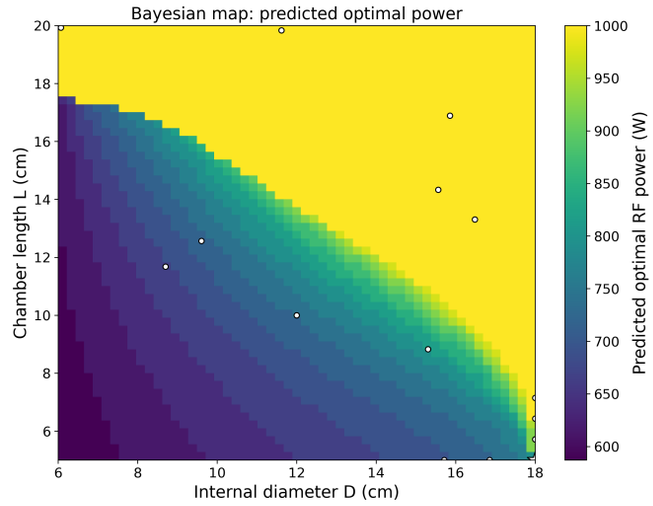


Fig. 2. Bayesian map of the RF power predicted to maximize the Child–Langmuir-limited thrust for each geometry

This result highlights the importance of incorporating physically constrained performance metrics during optimization. Maximizing plasma production alone does not necessarily translate into higher usable thrust because extraction limits and downstream system losses become dominant at elevated operating conditions. The application of correction layers therefore transforms the optimization process from a purely numerical exercise into a more realistic engineering assessment.

An additional consequence of the optimization process is that the maximum plasma-generation condition does not coincide with the maximum realistic-thrust condition. While higher RF power increases ion production and improves discharge sustainment, extraction limitations progressively decouple internal plasma performance from externally delivered thrust.

The shift of the optimum after applying engineering corrections therefore indicates that practical ion-thruster design requires simultaneous consideration of plasma generation, extraction capability, and subsystem efficiencies rather than isolated maximization of discharge conditions.

After application of the realistic system-level penalty, the best sampled point remained at the boundary of the explored design space, $D = 18.0\,\mathrm{cm}$ and $L = 5.0\,\mathrm{cm}$, but shifted to $P_{RF} = 1000\,\mathrm{W}$. The realistic thrust reached $45.0\,\mathrm{mN}$, exactly at the adopted cap of $45.0\,\mathrm{mN/kW}$. By contrast, the nominal-like configuration ($D = 12.0\,\mathrm{cm}$, $L = 10.0\,\mathrm{cm}$, $P_{RF} \approx 900\,\mathrm{W}$) produced a realistic thrust of $20.0\,\mathrm{mN}$, equivalent to $22.2\,\mathrm{mN/kW}$. These numbers suggest that the optimization framework is valuable for ranking configurations, but that system-level penalties are indispensable for meaningful comparisons with flight-like devices. Table IV summarizes these four representative design points — nominal-like, geometry-only, Child–Langmuir-limited, and realistic — for direct comparison.

The commercial comparison supports this interpretation. Table V lists the power, thrust, and thrust-to-power figures used for this benchmark. ArianeGroup's RIT 10 EVO spans 5–25 mN over 145–760 W [5], while the RIT 2X [5], QinetiQ T6 [6], and NASA NEXT [7] extend the gridded-ion-engine

envelope to higher powers and larger thrusts. The penalized predictions from the present model cluster inside, or at the upper edge of, the practical thrust-to-power band usually associated with gridded ion engines. Therefore, the methodology is well suited for preliminary design exploration, even though additional physics—such as plume divergence, charge-exchange losses, grid lifetime, and thermal constraints—must be added before using the model as a predictive engineering tool. Fig. 3 places the raw, Child–Langmuir-limited, and realistic penalized predictions alongside the RIT, QinetiQ, and NASA NEXT benchmark points, showing that the penalized results fall within the typical $25\text{–}45\,\mathrm{mN/kW}$ envelope for gridded ion engines.

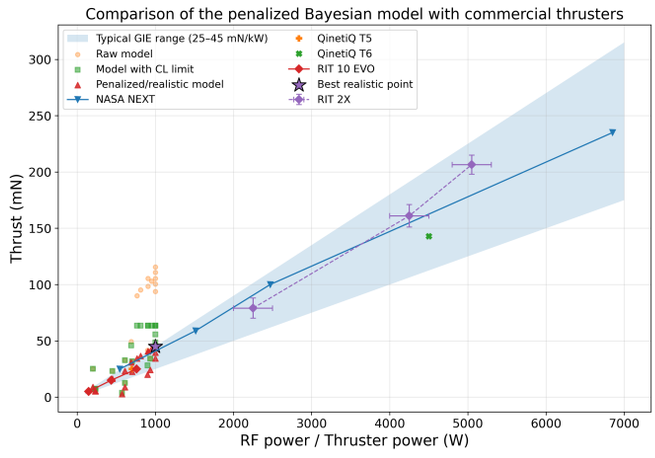


Fig. 3. Comparison between raw, Child–Langmuir-limited, and realistic penalized model predictions and representative commercial ion thrusters.

Table IV

REPRESENTATIVE OPTIMIZATION OUTCOMES

| Case | $D$ (cm) | $L$ (cm) | $P_{RF}$ (W) | Thrust (mN) |
|---|---|---|---|---|
| Nominal-like | 12.0 | 10.0 | 900 | 20.0 |
| Best geometry-only | 18.0 | 5.0 | 900 | 104.9 |
| Best CL-limited | 18.0 | 5.0 | 765 | 63.6 |
| Best realistic | 18.0 | 5.0 | 1000 | 45.0 |

Table V

COMMERCIAL BENCHMARK POINTS USED FOR COMPARISON

| Thruster | Power (W) | Thrust (mN) | mN/kW |
|---|---|---|---|
| RIT 10 EVO | 145–760 | 5–25 | 33–35 |
| RIT 2X | 2000–5300 | 70–215 | 35–41 |
| QinetiQ T5 | 700 | 25 | 35.7 |
| QinetiQ T6 | 4500 | 143 | 31.8 |
| NASA NEXT | 545–6853 | 25–235 | 34–46 |

## IV. CONCLUSION

A corrected global model combined with Bayesian optimization successfully captured the main design trends of an RF inductively coupled gridded argon ion thruster. Larger reactor diameters and shorter lengths were consistently favored.

Although the raw model predicted very high thrust in the most aggressive operating regime, the Child–Langmuir limit and the realistic engineering penalty substantially moderated these values. The resulting best realistic point was $45\,\mathrm{mN}$ at $1\,\mathrm{kW}$, which places the optimized design at the upper boundary of a reasonable gridded-ion-engine performance envelope. The results also indicate that argon can constitute a viable low-cost alternative for RF gridded ion propulsion, particularly when efficient ionization pathways associated with excited and metastable states are exploited. The proposed workflow demonstrates that reduced-order plasma models combined with Bayesian optimization can provide physically meaningful guidance during early-stage thruster development. The inclusion of excited-state argon chemistry, extraction constraints, and engineering penalties enables the model to connect internal plasma behavior with realistic propulsion performance, providing a practical framework for preliminary electric propulsion design.

## REFERENCES

[1] D. M. Goebel and I. Katz, *Fundamentals of Electric Propulsion: Ion and Hall Thrusters*. Hoboken, NJ, USA: Wiley, 2008.

[2] B. Magaldi, J. Karnopp, A. da Silva Sobrinho, and R. Pessoa, ”A global model study of plasma chemistry and propulsion parameters of a gridded ion thruster using argon as propellant,”*Plasma*, vol. 5, no. 3, pp. 324–340, 2022.

[3] M. A. Lieberman and A. J. Lichtenberg, *Principles of Plasma Discharges and Materials Processing*, 2nd ed. New York, NY, USA: John Wiley & Sons, 2005.

[4] C. E. Rasmussen and C. K. I. Williams, *Gaussian Processes for Machine Learning*. Cambridge, MA, USA: MIT Press, 2006.

[5] ArianeGroup, ”Spacecraft Propulsion with Thrust and Precision into Space,”product brochure, 2019.

[6] J. S. Snyder, D. M. Goebel, R. R. Hofer, J. E. Polk, N. C. Wallace, et al., ”Performance Evaluation of the T6 Ion Engine,”AIAA/ASME/SAE/ASEE Joint Propulsion Conference, 2010.

[7] NASA, ”NASA’s Evolutionary Xenon Thruster (NEXT) – Thruster Data Sheet and Guidebook,”Discovery AO Library, 2014.

[8] P. Chabert et al., ”Global model of a gridded-ion thruster powered by a radiofrequency inductive coil,”*Physics of Plasmas*, vol. 19, no. 7, Art. no. 073512, 2012.

[9] H. M. Nussenzveig, *Curso de Física Básica, vol. 2: Fluidos, Oscilações e Ondas, Calor*, 2nd ed. São Paulo, Brazil: Blucher, 2014.

[10] H. M. Nussenzveig, *Curso de Física Básica, vol. 3: Eletromagnetismo*, 2nd ed. São Paulo, Brazil: Blucher, 2015.

[11] P. N. Randall, R. A. Lewis, and S. D. Clark, ”QinetiQ T5 based Electric Propulsion System and Architectural Options for Future Applications,”IEPC-2017-170, 2017.